Dual-frequency capacitive discharges: Effect of low-frequency current on electron distribution function

H. C. Kim and J. K. Lee[a)]
Department of Electronic and Electrical Engineering, Pohang University of Science and Technology, Pohang 790-784, Republic of Korea

(Received 18 January 2005; accepted 22 February 2005; published online 7 April 2005)

In low-pressure dual-frequency capacitive discharges, the effect of the low-frequency current on the electron distribution function (EDF) was investigated through the particle-in-cell simulation with Monte Carlo collision model. As the low-frequency (2 MHz) current increases for the fixed high-frequency (27 MHz) current, the EDF changes from Druyvesteyn to bi-Maxwellian (in the absence of secondary electron emission) or Maxwellian type (in case with secondary electron emission), along with the significant drop in the effective electron temperature. When the role of secondary electron emission is negligible, the EDF transition is attributed to the transition from collisional to collisionless property (but not stochastic heating) of the low-energy electrons. The Ramsauer minimum which makes low-energy electrons less collisional plays an important role in making this transition as well as in determining the spatial electric field structure. When the role of secondary electron emission is significant, the transition is attributed to the α-γ transition. © *2005 American Institute of Physics*. [DOI: 10.1063/1.1888325]

I. INTRODUCTION

Capacitively coupled rf discharges have been extensively studied for the last decades because of their interesting physics as well as their widespread applications.[1] Concerning the sustainment of capacitively coupled rf discharges, several types of discharge transitions have been reported. Both transitions are accompanied by the changes in the electron distribution function (EDF) and the effective electron temperature. Godyak and Piejak[2] observed the EDF change from Druyvesteyn to bi-Maxwellian type with decreasing argon gas pressure. They explained that the abnormally low electron temperature and the observed transition are attributed to a change from collisional to stochastic electron heating enhanced by the Ramsauer effect. However, Kaganovich and Tsendin[3] showed that the observed transition can be explained by the nonlocal electron kinetics in inhomogeneous rf field even without accounting for the stochastic heating. When the half of the discharge dimension is much less than the energy relaxation length, electrons are in the nonlocal regime. The EDF is not determined only by the local electric field but is also dependent on the electric field at other positions where electrons can reach. The electrons are trapped by the potential well formed by the ambipolar potential and the accessible volume of the electrons depends on their energies. The temperature of low-energy electrons at the discharge center is very low since they are confined in the low rf field region by the dc ambipolar potential barrier. The high-energy electrons at the discharge center can penetrate into the high rf field region and hence the temperature of high-energy electrons is higher than that of low-energy electrons. The other type is the transition from the low-voltage (or α) to the high-voltage (or γ) mode with increasing discharge current density.[4] At the low rf voltage the ionization is provided by the bulk plasma electrons, while at the high voltage the ionization is maintained by the secondary electrons injected from the electrodes due the ion bombardment. Even when the role of the secondary electrons is negligible, the mode transition while varying the current has been reported.[5,6] Berezhnoi *et al.*[5] interpreted its mechanism as an anology of a thermal explosion. However, most of previous works on discharge transitions have been limited only to the conventional capacitively coupled plasma (CCP) with a single rf (13.56 MHz) source. Recently, dual frequency (DF) CCP operated with one more power supply than the conventional CCP has attracted much attention due to its advantage of the independent control of the ion flux and ion bombardment energy onto the electrodes.[7–12] Since the contributions of high-frequency and low-frequency sources to the plasma are generally coupled to each other, it is important to find the regime where the ion flux and ion bombardment energy can be independently controlled. In this control, it is important to understand how the low-frequency source affects the electron temperature (and hence the ion flux).

In this paper, we investigate the effect of the low-frequency current on the EDF in DF CCP as an extension of the earlier study in Ref. 12. Section II deals how effective frequencies for generalized Ohm's law are defined and obtained. Section III shows the particle-in-cell/Monte Carlo collision (PIC-MCC) simulation result for four cases with and without secondary electron emission (SEE) at the wall and Ramsauer minimum in elastic scattering cross section. Finally, our works are summarized in Sec. IV.

II. EFFECTIVE FREQUENCIES FOR GENERALIZED OHM'S LAW

The current is related to the electric field by the classical Ohm's law as follows:[1]

[a)]Electronic mail: jkl@postech.ac.kr

$$\tilde{J} = \sigma_p \tilde{E}, \tag{1}$$

with the plasma conductivity

$$\sigma_p = \frac{\varepsilon_0 w_{\mathrm{pe}}^2}{\nu_m + jw}, \tag{2}$$

where $\varepsilon_0 = 8.85 \times 10^{-12}$ F m^{-1} and w_{pe} are the permittivity of free space and the electron plasma frequency, respectively. The electron collision frequency for momentum transfer ν_m is defined as

$$\nu_m = \frac{1}{n_e} \int_0^\infty \nu_{\mathrm{mt}}(\varepsilon) \varepsilon^{1/2} g(\varepsilon) d\varepsilon, \tag{3}$$

where $\nu_{\mathrm{mt}}(\varepsilon)$ is energy-dependent collision frequency for momentum transfer and $g(\varepsilon)$ is the electron energy probability function. According to the Ohm's law, the change of the electric field for the fixed current density comes from the change of plasma frequency, collision frequency, or applied frequency. However, the classical Ohm's law of Eqs. (1) and (2) is valid only under the limited condition.

The general relation between the rf electric field and rf current density (generalized Ohm's law) is defined as follows:

$$\tilde{J} = \sigma_e \tilde{E}, \tag{4}$$

with the generalized form of the plasma conductivity

$$\sigma_e \equiv \frac{\varepsilon_0 w_{\mathrm{pe}}^2}{\nu_{\mathrm{eff}} + j w_{\mathrm{eff}}}. \tag{5}$$

The effective frequencies ν_{eff} and w_{eff} replace the frequencies ν_m and w included in the classical conductivity of Eq. (2). To consider the non-Maxwellian EDF, we define different frequencies, ν_{en} and w' as follows:[13]

$$\sigma_e' = \frac{\varepsilon_0 w_{\mathrm{pe}}^2}{\nu_{\mathrm{en}} + jw'} = -\frac{2}{3n_e} \varepsilon_0 w_{\mathrm{pe}}^2 \int_0^\infty \frac{\varepsilon^{3/2}}{\nu_{\mathrm{mt}}(\varepsilon) + jw} \frac{dg}{d\varepsilon} d\varepsilon. \tag{6}$$

The collision frequency ν_m is not the same as ν_{en}, when the EDF is not Maxwellian or the collision frequency is not constant for electron energy. The values of ν_{eff} and w_{eff} are defined from the plasma resistivity,[14]

$$\rho = \tilde{E} \cos\psi / \tilde{J} = \mathrm{Re}(\sigma_e^{-1}) = m\nu_{\mathrm{eff}} / ne^2 \tag{7}$$

and plasma reactance

$$\xi = \tilde{E} \sin\psi / \tilde{J} = \mathrm{Im}(\sigma_e^{-1}) = m w_{\mathrm{eff}} / ne^2, \tag{8}$$

where m is the electron mass, n is the plasma density, and ψ is the phase shift between the rf electric field $\tilde{E}$ and the rf current density $\tilde{J}$. The frequencies ν_{en} and ν_{eff} are not the same, when there is significant collisionless (or non-Ohmic) power absorption or electrons are not in local equilibrium.[14,15] Thus, the discrepancy between (ν_{en}, w') and (ν_{eff}, w_{eff}) indicates that the nonlocality in electron kinetics plays an important role. When the amplitude and phase for the current density and electric field are known, the effective frequencies can be calculated from Eqs. (7) and (8). Since the EDF in the bulk plasma region is governed by the high-frequency field rather than the low-frequency one, the effective frequencies only for the high-frequency source will be calculated.

When the current density and electric field are assumed to be expressed as

$$A(t) = a_0 + \sum_{n=1}^{\infty} a_{h,n} \cos(n w_h t + \phi_{h,n}) + \sum_{n=1}^{\infty} a_{l,n} \cos(n w_l t + \phi_{l,n}), \tag{9}$$

the amplitude and phase of the high-frequency (w_h) component of $A(t)$ can obtained by the following formula:

$$a_{h,1} = \sqrt{2[\langle A(t)\cos(w_h t)\rangle^2 + \langle A(t)\sin(w_h t)\rangle^2]} \tag{10}$$

and

$$\phi_{h,1} = \arctan\left(\frac{\langle A(t)\sin(w_h t)\rangle}{\langle A(t)\cos(w_h t)\rangle} \right), \tag{11}$$

where $\langle \cdot \rangle$ means averaging over the rf period. Equations (10) and (11) are used to obtain the amplitude and phase for the current density and electric field from their time-dependent values.

III. PIC-MCC SIMULATION

For this study, we have used a one-dimensional electrostatic PIC simulation method with MCC model[16–18] which is a self-consistent and fully kinetic method. In the simulation, the ground state argon gas density is assumed to remain constant and uniform in space. The motion of atoms in excited states and Coulomb collisions between charged particles are not considered. Collisional effects are included by coupling PIC method with MCC technique.[17] For electrons colliding with neutrals, the elastic scattering, excitation, and ionization are taken into account. For argon ions colliding with neutrals, charge exchange and elastic scattering are considered. Since PIC-MCC simulation makes no assumption on velocity distribution, it yields important information on the electron and ion energy distribution function. This method is particularly useful in modeling low-pressure rf discharge where the EDF is not in equilibrium with the local electric field (which is called nonlocal regime). Our simulations were performed for argon discharges with two parallel-plate electrodes separated by the gap distance of 2.5 cm. Operating gas pressure was 100 mTorr. Two rf current sources with frequencies of 27 MHz ($=w_h$) and 2 MHz ($=w_l$) were applied to the powered electrode at position $x=0$ cm. The electric potential at the boundary is found by applying the continuity of current.[18] The amplitude of the high-frequency (27 MHz) current was fixed at 1 mA cm^{-2} while the low-frequency (2 MHz) current was varied in the range of 0–0.3 mA cm^{-2}. The electrode at position $x=2.5$ cm was grounded. For the stability and accuracy of the PIC-MCC simulation,[16,19] we used 400 cells and the time step of 4×10^{-12} s. To obtain the meaningful result at the steady state, we performed the simulation runs for several thousand rf cycles. To suppress the statistical noise sufficiently, the total number of superparticles for electrons (or ions) at the steady state is made to be larger than 1.5×10^5. In single-frequency CCP, the simula-

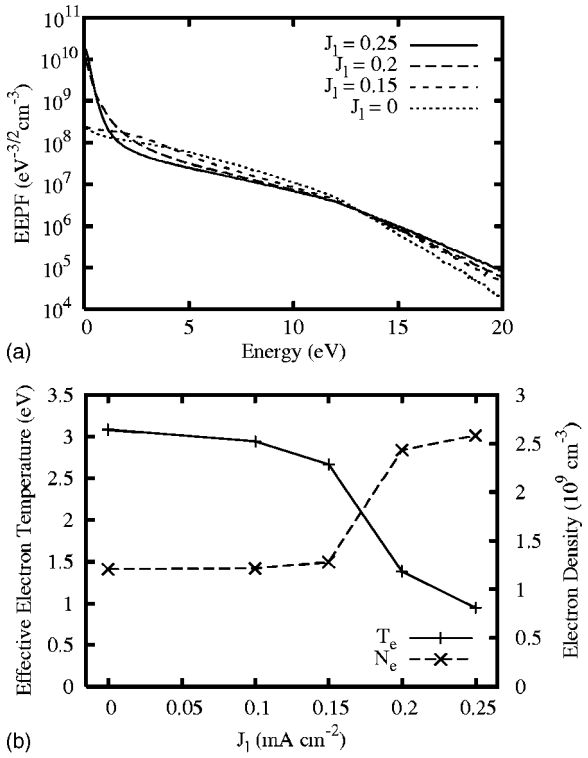

FIG. 1. Simulation result without SEE: (a) Electron energy probability functions at the discharge center for various low-frequency currents. (b) Effective electron temperature and electron density at the discharge center as a function of the low-frequency current. Time-averaged values were presented.

tion result obtained by using our code agrees well with experimental data.[20] The SEE coefficients due to the electron or ion impact are different for various electrode materials. Hence, both cases with and without the SEE are simulated. In case with the SEE, the SEE coefficient due to ion impact is set to 0.2 while the energy and angular dependence for electron impact secondary yield is considered.[21,22] The energy and angular distribution of emitted secondary electrons[23] are also considered. In our result, the effective electron temperature is defined as

$$T_{\text{eff}} = \frac{2}{3n_e} \int \varepsilon^{3/2} g(\varepsilon) d\varepsilon. \tag{12}$$

A. Simulation without SEE

For the case without the SEE, the EDFs calculated at the discharge center for different low-frequency currents are shown in Fig. 1(a). As the low-frequency current increases, it changes from Druyvesteyn to bi-Maxwellian type. In bi-Maxwellian distribution, the temperature of high-energy electrons is larger than that of low-energy electrons. In Druyvesteyn distribution, the temperature of low-energy electrons is larger than that of high-energy electrons. The temperature of low-energy electrons decreases with the low-frequency current while the tail temperature increases. As shown in Fig. 1(b), the effective electron temperature at the discharge center decreases with the low-frequency current along with the small increase of the electron density. The

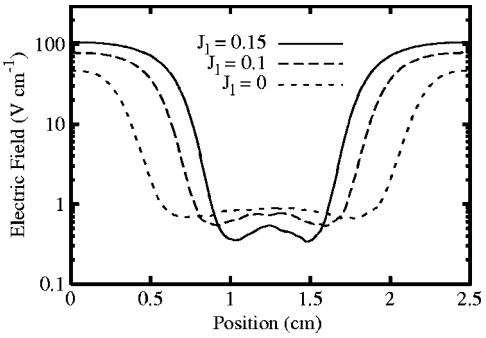

FIG. 2. Simulation result without SEE. The spatial profiles of the rms rf electric field for different low-frequency currents.

discharge is not sustained for much higher low-frequency current above 0.25 mA cm^{-2} because of the significant decrease of the bulk plasma (where electron and ion densities are the same) width.[10] The effective electron temperature is mostly determined by the electrons having energy in elastic range. At the gas pressure of 100 mTorr with the gap distance $2L = 2.5$ cm, since half of the gap distance is much less than the energy relaxation length λ_ε for the electrons in elastic energy range ($\lambda_\varepsilon \gg L$), these electrons are in the nonlocal regime.[3] The electrons are trapped by the potential well formed by the ambipolar potential and the accessible volume of the electrons depends on their energies. The EDF is mainly affected by the spatial inhomogeneity of the electric field, the sheath heating, and the Ramsauer effect.[24]

In CCP, the electrons gain energy from the electric field. Figure 2 shows the spatial profiles of the rms rf electric field for different low-frequency currents. Since the electron plasma frequency is larger than applied frequencies, the electric field is strongly shielded from the bulk of the plasma. The electric field at the discharge center decreases with the low-frequency current while the field at the sheath increases. The low-energy electrons are trapped near the discharge center but the high-energy electrons can reach the sheath region. Thus, the temperature of the low-energy electrons decreases while the tail temperature increases as shown in Fig. 1(a). The inhomogeneity of the electric field increases with the low-frequency current. This inhomogeneous electric field structure leads to the bi-Maxwellian EDF since higher-energy electrons are accessible to the regions of higher rf field strength. It is also interesting that the electric field structure is not monotonic near bulk-sheath boundaries for some low-frequency currents. A similar phenomenon was observed in inductively coupled plasmas.[25,26] It was interpreted in terms of the anomalous skin effect. The nonlinear effect in the capacitive sheath with deep radio frequency electric field penetration is also found in Ref. 27.

Figures 3(a)–3(c) show the spatial profile of the power consumed by electrons for low-frequency currents of 0, 0.15, and 0.2 mA cm^{-2}, respectively. The total electron power $P_{e,\text{tot}}(\equiv\langle J_e E\rangle)$ is the same as the sum of the high-frequency electron power $P_{e,h}$ ($\equiv J_{e,h} E_h \cos(\psi_h)/2$), low-frequency electron power $P_{e,l}$ ($\equiv J_{e,l} E_l \cos(\psi_l)/2$), and dc electron power $P_{e,\text{dc}}$ ($\equiv\langle J_e\rangle\langle E\rangle$). The dc electron power is negative since it comes from the electron cooling due to electron

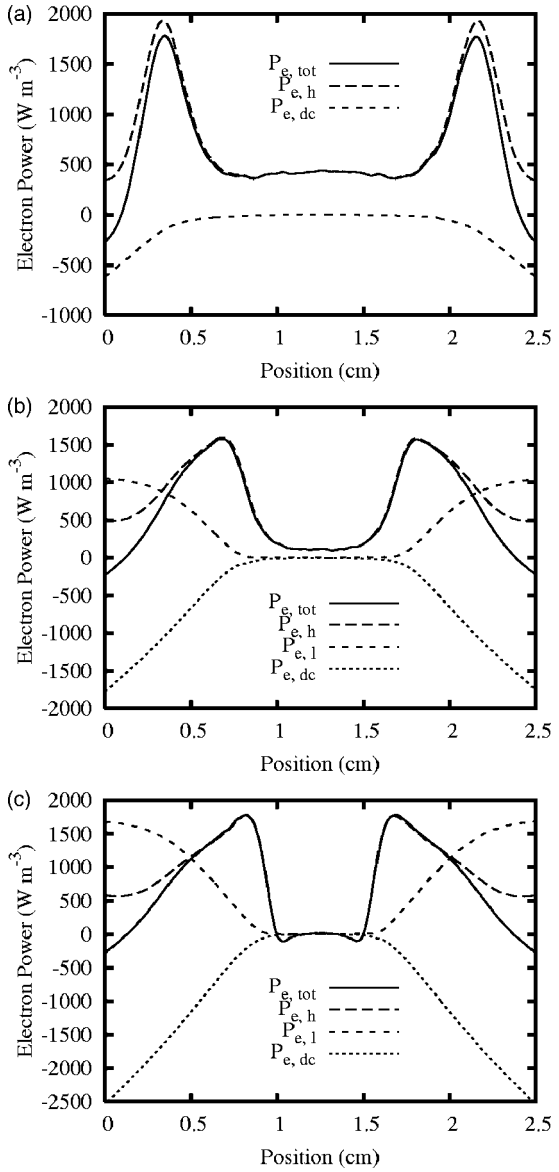

FIG. 3. Simulation result without SEE. The spatial profile of the power consumed by electrons for low-frequency currents of (a) 0, (b) 0.15, and (c) 0.2 mA cm^{-2}.

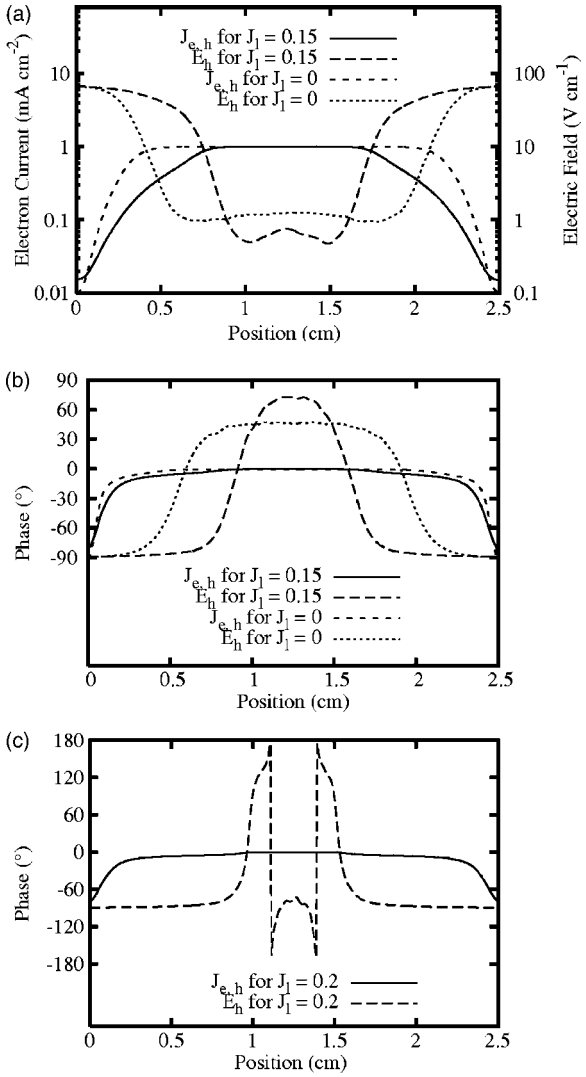

FIG. 4. Simulation result without SEE: (a) The amplitude and (b) phase of the high-frequency component of the electron current density and electric field for low-frequency currents of 0 and 0.15 mA cm^{-2}. (c) The phase of the high-frequency component of the electron current density and electric field for the low-frequency current of 0.2 mA cm^{-2}.

losses to electrodes. The absolute values of the low-frequency electron power and dc electron power are largest near electrodes while the high-frequency power is largest near bulk-sheath boundaries. The absolute values of the low-frequency power and dc power increase with the low-frequency current. However, since the signs of two powers are opposite, they cancel out. Hence, the electron power is mainly contributed from the high-frequency electron power. Nevertheless, the low-frequency source can affect the spatial profile of the high-frequency electron power. The electron power in the bulk decreases with the low-frequency current. For the low-frequency current above 0.15 mA cm^{-2}, the electron power near bulk-sheath boundaries becomes even negative [Fig. 3(c)]. The negative power means that the phase shift between the electric field and electron current is larger than 90°. For better understanding, the amplitude and phase of the electron current density and electric field which determine the electron power are also calculated.

Figure 4 shows the amplitude and phase of the high-frequency component of the electron current density and electric field for different low-frequency currents, which were obtained from the PIC-MCC simulation and Eqs. (10) and (11). Because of the current continuity, the high-frequency electron current in the discharge center is the same as the applied high-frequency current with the amplitude of 1 mA cm^{-2} and the phase of 0. The phase of the electric field and hence the phase shift ψ significantly change with low-frequency current [Figs. 4(b) and 4(c)]. The negative power near bulk-sheath boundaries is associated with the abrupt change in the phase of the electric field near bulk-sheath boundaries [Figs. 3(c) and 4(c)]. The similar phenomenon was reported in inductively coupled plasmas.[28]

Figures 5(a) and 5(b) show frequencies ν_{en}, w_{eff}, and ν_{eff} at the discharge center and the position of maximum electron power deposition, respectively. The effective frequencies

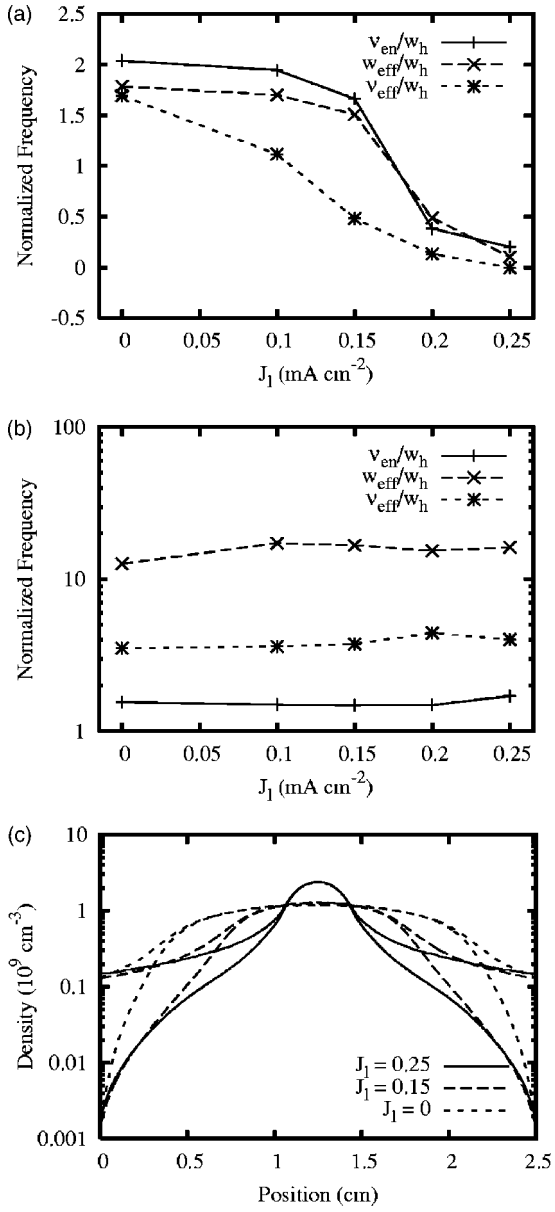

FIG. 5. Simulation result without SEE: Frequencies calculated at (a) the discharge center and (b) the position where the consumed power by electrons has the maximum value. (c) The spatial profiles of the ion and electron densities for low-frequency currents of 0, 0.15, and 0.25 mA cm^{-2}.

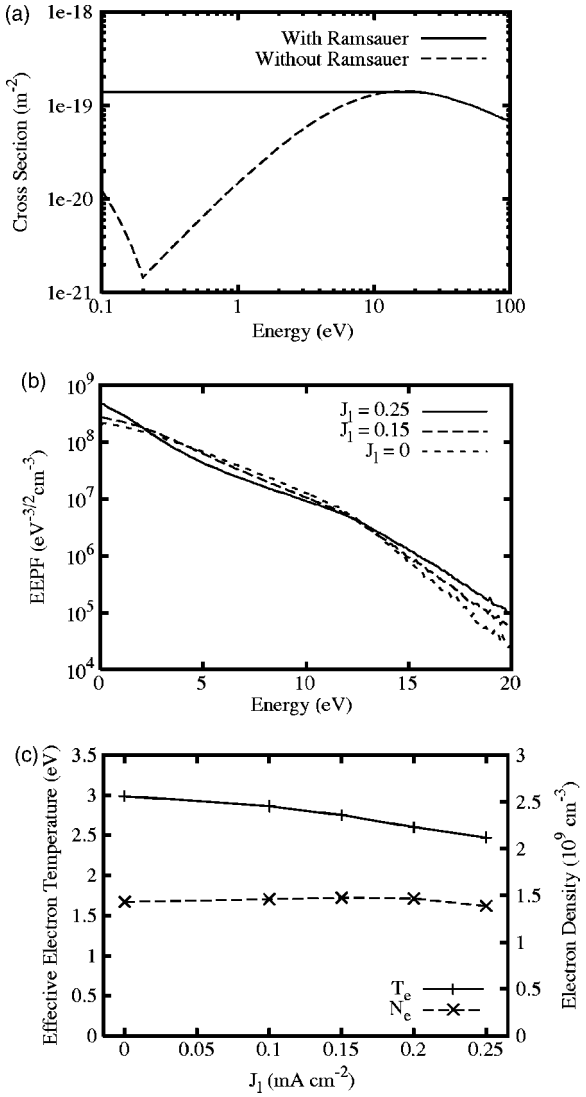

FIG. 6. Simulation result without SEE in the absence of the Ramsauer minimum: (a) Model elastic collision cross section. (b) Electron energy probability functions at the discharge center. (c) The electron temperature and electron density at the discharge center.

were obtained from the PIC-MCC simulations by using the way described in Sec. II. All frequencies are normalized to w_h. According to the generalized Ohm's law of Eq. (4) for the fixed high-frequency current, the change of the electric field is due to that of w_{pe}, ν_{eff}, or w_{eff}. It is noted from the comparison of the plasma density and the effective frequencies [Figs. 1(b) and 5(a)] that the change of the electric field at the discharge center is mainly due to two effective frequencies rather than the plasma density. The significant decrease of the frequencies can be interpreted as the transition from collisional to collisionless property of the low-energy electrons. For the argon gas, the electron mean free path for momentum transfer λ_e between 0.4 and 10 cm decreases with energy because of the Ramsauer minimum. As shown in Fig. 5(c), the plasma width $2d$ decreases with the low-frequency current because of the increase of the sheath width. As a result, the low-energy electrons become collisionless (since $\lambda_e \gg d$) and their temperature significantly decreases. This trend is quite opposite to the result of global model (volume-averaged fluid model) that the electron temperature increases with the decrease of the plasma width.[1] Unlike the results of Refs. 13 and 14, it is found from Fig. 5(a) that the values of ν_{eff}/ν_{en} and w_{eff}/w_h at the discharge center can also be smaller than unity, along with their anomalous decreases. Since the effective frequency ν_{eff} includes both of the collisional (ν_{en}) and collisionless effects, our result ($\nu_{eff} < \nu_{en}$) means that there is a significant collisionless effect which leads to electron cooling in the plasma bulk region. It is consistent with the result of Ref. 29 that the total electron heating at the discharge center is smaller than the Ohmic heating. It can arise from the nonlocal behavior of the electrons since the conductivity in the nonlocal regime has the different form with the classical conductivity.[15] It is therefore concluded that the EDF transition while changing

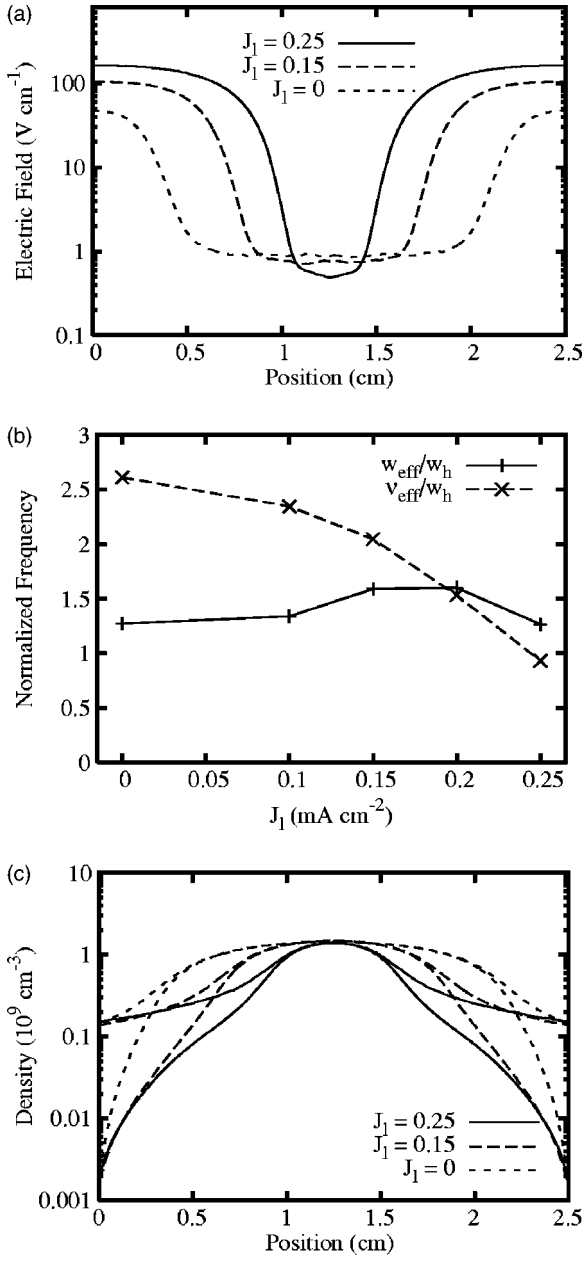

FIG. 7. Simulation result without SEE in the absence of the Ramsauer minimum: (a) The spatial profiles of the rms rf electric field. (b) Effective frequencies at the discharge center. (c) The spatial profiles of the ion and electron densities.

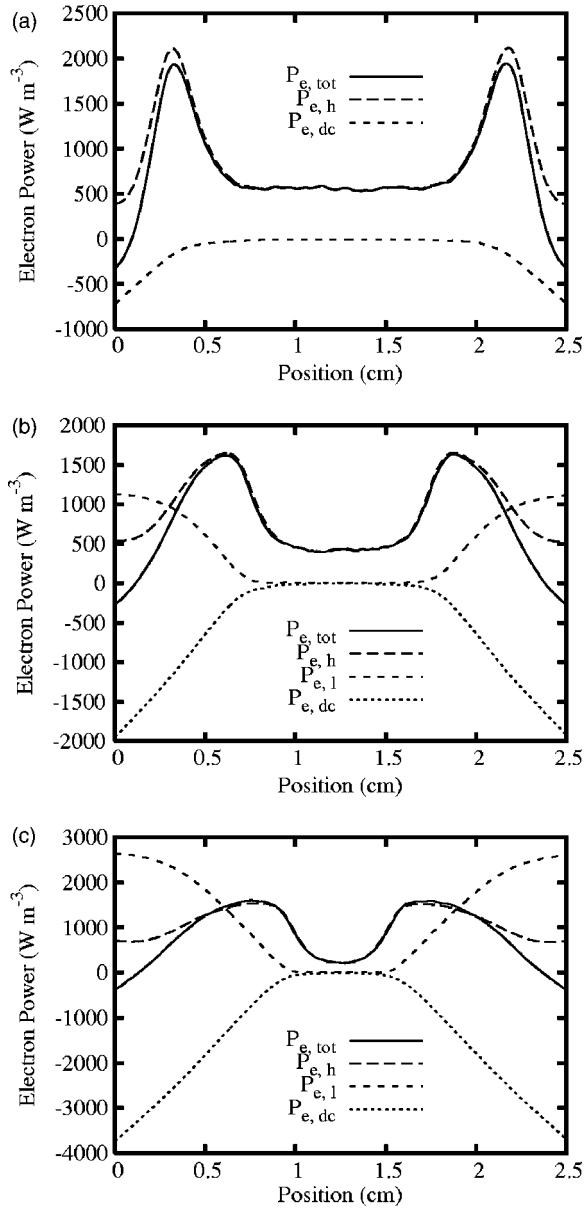

FIG. 8. Simulation result without SEE in the absence of the Ramsauer minimum: The spatial profile of the power consumed by electrons for low-frequency currents of (a) 0, (b) 0.15, and (c) 0.25 mA cm^{-2}.

the low-frequency current is attributed to the transition from collisional to collisionless property of the low-energy electrons. On the other hand, it is found from Fig. 5(b) that the effective frequencies in the region where stochastic heating (or sheath heating) is possible do not change much with the low-frequency current. Hence, the collisionless mechanism in our simulation is not attributed to stochastic heating which is the typical type of collisionless electron heating. According to Ref. 29, stochastic heating is not dominant electron heating mechanism even in 10 mTorr.

To investigate the effect of the Ramsauer minimum, the simulation with the removal of the Ramsauer minimum in elastic collision cross section was also performed in a similar way to Ref. 30. Figure 6(a) shows the model elastic collision cross section used for this simulation. When the Ramsauer minimum is turned off, the electrons become more collisional because of the increase in the collision cross section. It prevents the transition from collisional to collisionless property. In comparison with the case where the Ramsauer minimum is included, the EDFs do not change much with the low-frequency current as shown in Fig. 6(b). No abrupt change is shown in the effective electron temperature and electron density as shown in Fig. 6(c). In the low value of the low-frequency current, the Ramsauer effect on electron temperature and electron density is not significant [Figs. 1(b) and 6(c)]. Meanwhile, in the high value of the low-frequency current, the Ramsauer effect makes the significant changes in the electron temperature and electron density [Figs. 1(b) and 6(c)]. The EDF transition while varying the low-frequency current is observed only in the simulation where the Ram-

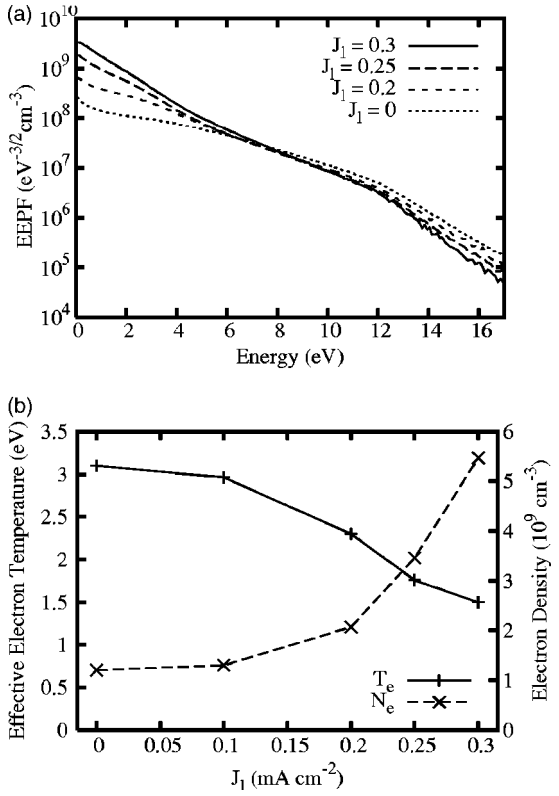

FIG. 9. Simulation result with SEE: (a) Electron energy probability functions at the discharge center for various low-frequency currents. (b) Effective electron temperature and electron density at the discharge center as a function of the low-frequency current.

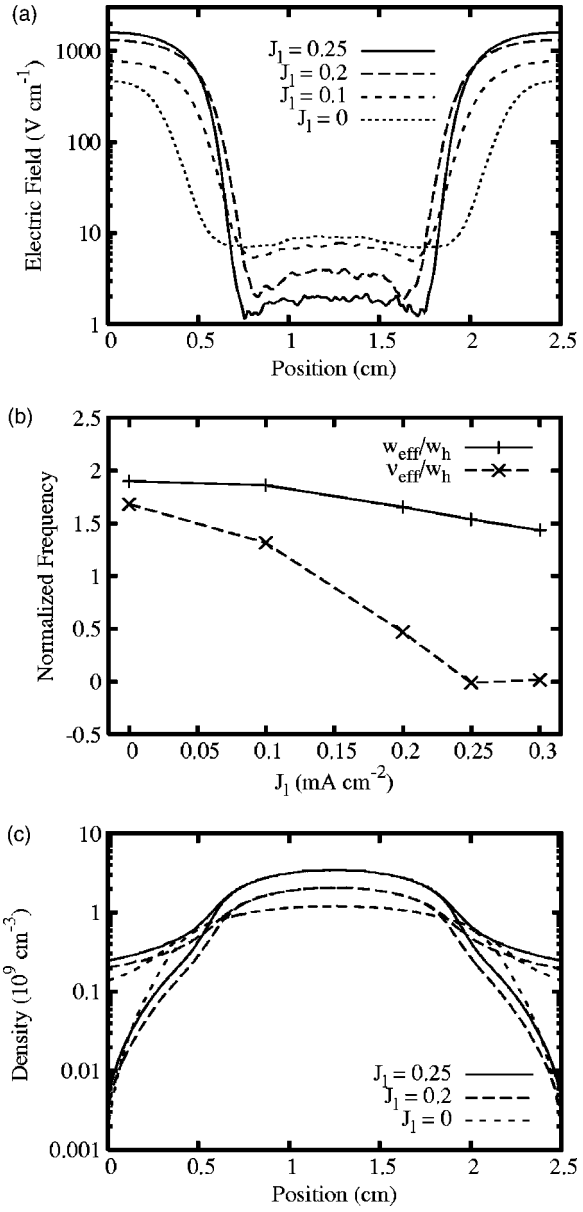

FIG. 10. Simulation result with SEE: (a) The spatial profiles of the rms rf electric field for different low-frequency currents. (b) Effective frequencies calculated at the discharge center. (c) The spatial profiles of the ion and electron densities for low-frequency currents of 0, 0.2, and 0.25 mA cm^{-2}.

sauer minimum is included [Figs. 1(a) and 6(a)]. Figure 7 shows the corresponding rf electric field, effective frequencies, and plasma density. As shown in Fig. 7(a), the nonmonotonic field structure does not appear in the absence of the Ramsauer minimum. Although the effective collision frequency at the discharge center and the plasma width decrease with the low-frequency current, they do not decrease as fast as that in case with the Ramsauer minimum [Figs. 5(a), 5(c), 7(b), and 7(c)]. The negative electron power near bulk-sheath boundaries is not also observed [Figs. 3(c) and 8]. Since the role of the Ramsauer minimum is to make low-energy electrons less collisional, it is concluded that the discharge transition and the nonmonotonic field structure are related to the collisionless property of low-energy electrons.

B. Simulation with SEE

The case with the SEE has also been investigated. The EDFs calculated at the discharge center for different low-frequency currents are shown in Fig. 9(a). As the low-frequency current increases, it changes from Druyvesteyn to Maxwellian type. As shown in Fig. 9(b), the effective electron temperature decreases with the low-frequency current. In comparison with the case without the SEE [Fig. 1(b)], there is a significant increase of the plasma density.

The spatial profiles of the rms rf electric field are shown in Fig. 10(a). As the low-frequency current increases, the electric field at the discharge center decreases and hence the inhomogeneity of the electric field increases. Figure 10(b) shows the effective frequencies w_{eff} and ν_{eff} at the discharge center. Unlike the case without the SEE, it is noted from the comparison of the plasma density and the frequencies [Figs. 9(b) and 10(b)] that the change of the electric field at the discharge center is mainly due to the plasma density rather than the frequencies. From the comparison of two cases with and without the secondary emission, it is noted that the EDF transition for the case with the SEE is associated with the α-γ transition.[4] As the low-frequency current increases, the sheath voltage increases and hence the SEE due to the ion impact becomes the dominant ionization process. Furthermore, emitted secondary electrons make efficient secondary ionization since they gain energy enough for the ionization through the sheath acceleration. The discharge is changed from the low-voltage to the high-voltage mode. Figure 10(c)

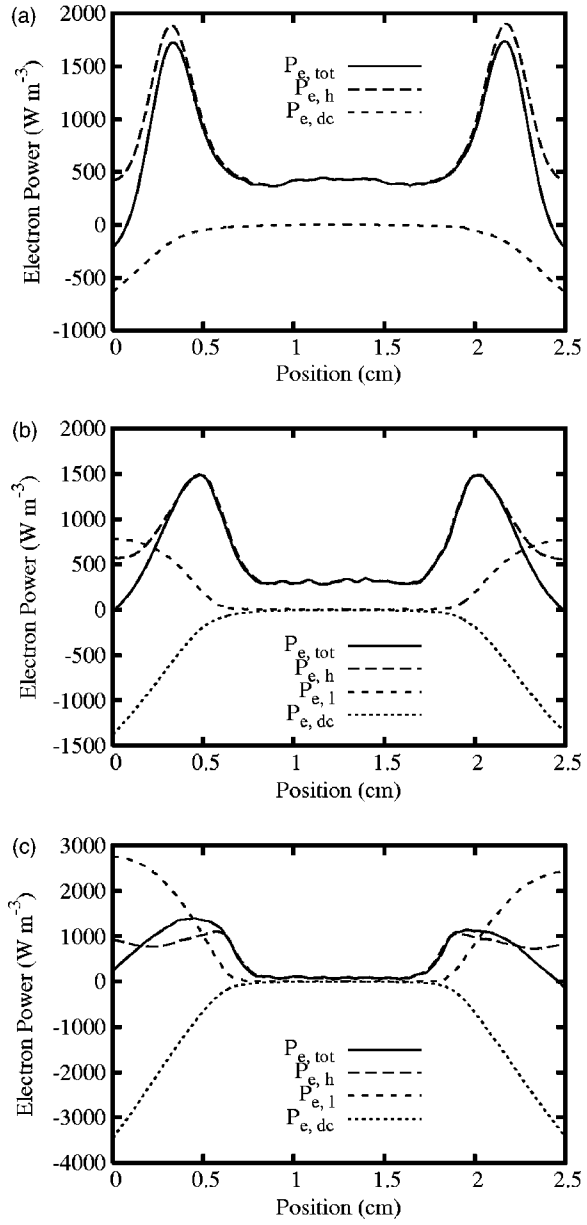

FIG. 11. Simulation result with SEE. The spatial profile of the power consumed by electrons for low-frequency currents of (a) 0, (b) 0.1, and (c) 0.2 mA cm^{-2}.

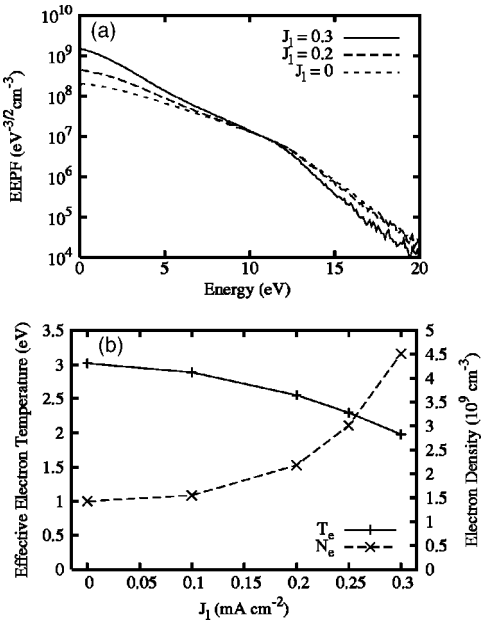

FIG. 12. Simulation result with SEE in the absence of the Ramsauer minimum: (a) Electron energy probability functions at the discharge center. (b) Effective electron temperature and electron density at the discharge center.

shows the spatial profile of the electron and ion densities for different low-frequency currents. When secondary electrons are in equilibrium with the local electric field, two peaks in the plasma density profile are observed in the high-voltage mode.[31] However, when secondary electrons are nonlocal, the plasma density has one peak at the discharge center even in the high-voltage mode, as reported in Ref. 32.

Figures 11(a)–11(c) show the spatial profile of the power consumed by electrons for low-frequency currents of 0, 0.1, and 0.2 mA cm^{-2}, respectively. In the absence of the SEE, the total electron power near electrodes is negative, as shown in Fig. 3. However, when the SEE is considered, the low-frequency electron power in the sheath increases more with the low-frequency current due to the additional heating of secondary electrons, and hence the total electron power near electrodes becomes positive for the low-frequency current above 0.1 mA cm^{-2}.

Figures 12–14 show the simulation results with the removal of the Ramsauer minimum for the case with the SEE. The transition while varying the low-frequency current is observed even in the absence of the Ramsauer minimum as shown in Fig. 12, unlike the case without the SEE. It is because the discharge transition for the case with the SEE is mainly attributed to the α-γ transition rather than the transition from collisional to collisionless property. Since the role of the SEE is more important than that of bulk electrons, the Ramsauer effect is not so significant as that in case without the SEE. However, it still plays a role to make the nonmonotonic rf field structure even in case with the SEE [Fig. 10(a) and 13(a)]. In the absence of the Ramsauer minimum, the effective frequencies also become less sensitive to the low-frequency current [Fig. 13(b)], like the case without the SEE.

IV. SUMMARY

The effect of the low-frequency current on the EDF was investigated in argon DF capacitive discharges through the PIC-MCC simulation. As the low-frequency (2 MHz) current increases for the fixed high-frequency (27 MHz) current, the EDF changes from Druyvesteyn to bi-Maxwellian type (in α mode) or Maxwellian type (in γ mode), along with the significant drop in the effective electron temperature. The electric field at the discharge center decreases with the low-frequency current and hence the inhomogeneity of the electric field increases. For some low-frequency currents, the spatial profile of the electric field was found to be nonmonotonic near bulk-sheath boundaries. From the PIC/MCC simulation, the amplitude and phase of the high-frequency component of the current density and electric field was obtained.

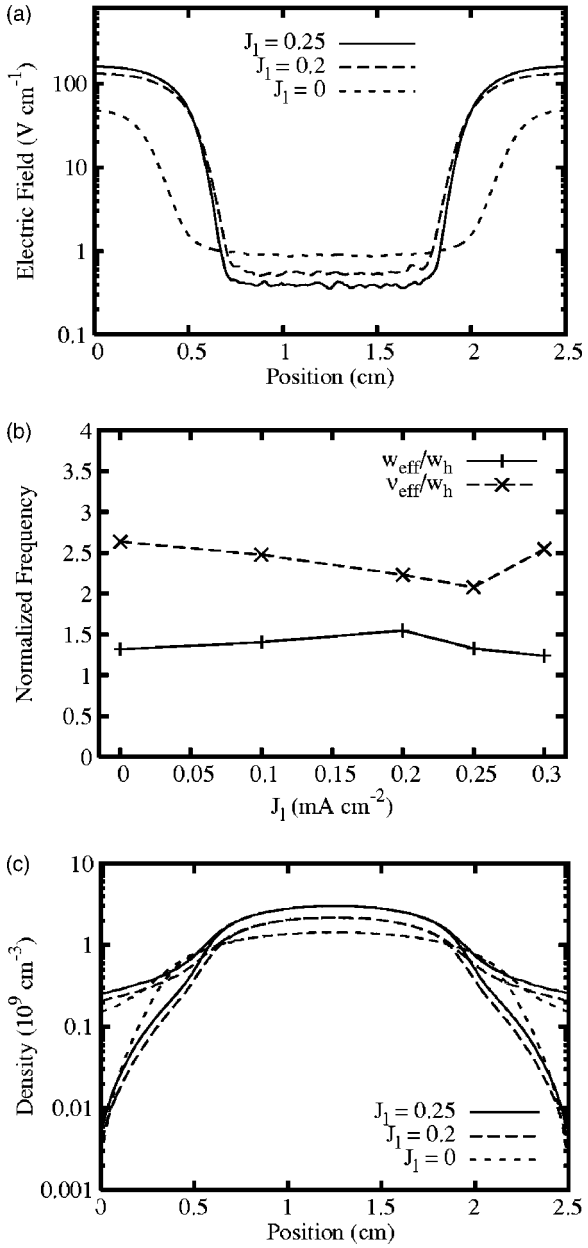

FIG. 13. Simulation result with SEE in the absence of the Ramsauer minimum: (a) The spatial profiles of the rms rf electric field. (b) Effective frequencies calculated at the discharge center. (c) The spatial profiles of the ion and electron densities.

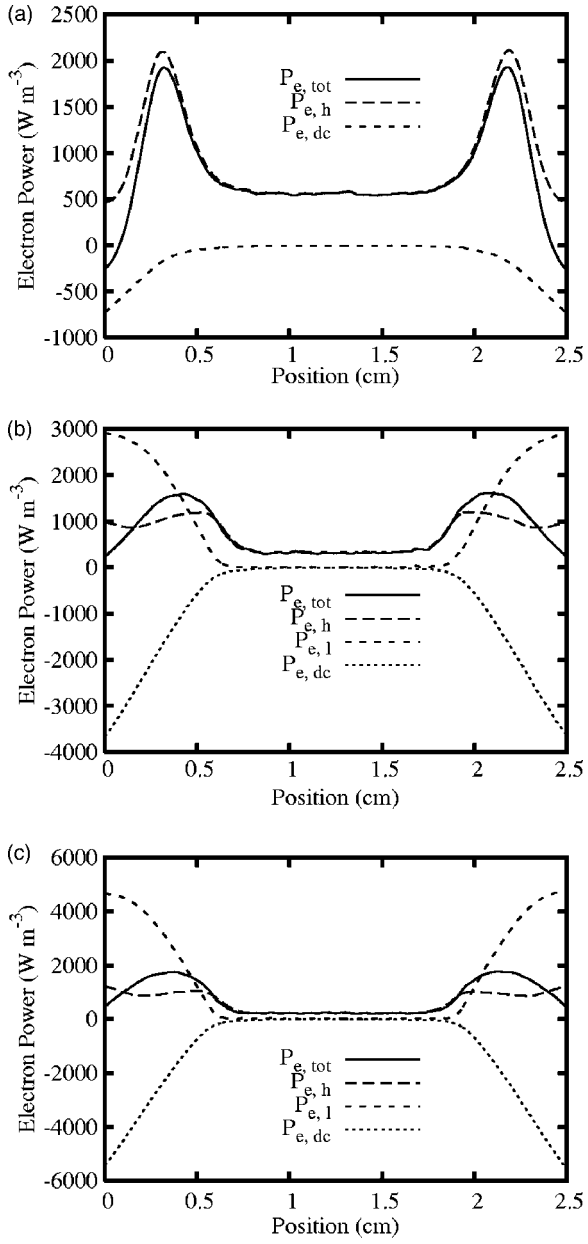

FIG. 14. Simulation result with SEE in the absence of the Ramsauer minimum. The spatial profile of the power consumed by electrons for low-frequency currents of (a) 0, (b) 0.2, and (c) 0.25 mA cm^{-2}.

By applying the generalized Ohm's law, the effective frequencies ν_{eff} and w_{eff} were obtained for various low-frequency currents. Depending on the magnitude of the SEE due to the ion bombardment, the mechanism for the EDF change is different. (a) When the role of the SEE is negligible, the decrease of the electric field at the discharge center is mainly due to anomalous decreases of two effective frequencies rather than the increase of the plasma density. The EDF transition while changing the low-frequency current is attributed to the transition from collisional to collisionless property of the low-energy electrons. In this transition, the Ramsauer minimum which makes low-energy electrons less collisional plays an important role. The transition is not related to stochastic heating which is the typical type of collisionless electron heating. (b) When the role of the SEE is significant, the decrease of the electric field at the discharge center is mainly due to the increase of the plasma density rather than the decreases of the frequencies. The EDF transition is attributed to the transition from the low-voltage (or α) to the high-voltage (or γ) mode.

ACKNOWLEDGMENTS

The authors greatly appreciate helpful discussions with Professor M. A. Lieberman at the University of California at Berkeley and Dr. N. Yu. Babaeva.

This work was supported in part by the Lam Research Corporation, Samsung Electronics, and Teralevel Nano Devices Project, 21c Frontier R&D Program in Korea Ministry of Science and Technology.

[1]M. A. Lieberman and A. J. Lichtenberg, *Principles of Plasma Discharges and Materials Processing* (Wiley, New York, 1994).
[2]V. A. Godyak and R. B. Piejak, Phys. Rev. Lett. **65**, 996 (1990).
[3]I. D. Kaganovich and L. D. Tsendin, IEEE Trans. Plasma Sci. **20**, 66 (1992).
[4]V. A. Godyak, R. B. Piejak, and B. M. Alexandrovich, Phys. Rev. Lett. **68**, 40 (1992).
[5]S. V. Berezhnoi, I. D. Kaganovich, and L. D. Tsendin, Plasma Phys. Rep. **24**, 556 (1998).
[6]I. V. Schweigert, Phys. Rev. Lett. **92**, 155001 (2004).
[7]T. Kitajima, Y. Takeo, Z. L. Petrovic, and T. Makabe, Appl. Phys. Lett. **77**, 489 (2000).
[8]S. Rauf and M. J. Kushner, IEEE Trans. Plasma Sci. **27**, 1329 (1999).
[9]P. C. Boyle, A. R. Ellingboe, and M. M. Turner, J. Phys. D **37**, 697 (2004).
[10]H. C. Kim, J. K. Lee, and J. W. Shon, Phys. Plasmas **10**, 4545 (2003).
[11]J. K. Lee, N. Babaeva, H. C. Kim, O. Manuilenko, and J. W. Shon, IEEE Trans. Plasma Sci. **32**, 47 (2004).
[12]H. C. Kim and J. K. Lee, Phys. Rev. Lett. **93**, 085003 (2004).
[13]G. G. Lister, Y.-M. Li, and V. A. Godyak, J. Appl. Phys. **79**, 8993 (1996).
[14]V. A. Godyak, R. B. Piejak, and B. M. Alexandrovich, J. Appl. Phys. **85**, 3081 (1999).
[15]B. Ramamurthi, D. J. Economou, and I. D. Kaganovich, Plasma Sources Sci. Technol. **12**, 302 (2003).
[16]C. K. Birdsall, IEEE Trans. Plasma Sci. **19**, 65 (1991).
[17]V. Vahedi and M. Surendra, Comput. Phys. Commun. **87**, 179 (1995).
[18]J. P. Verboncoeur, M. V. Alves, V. Vahedi, and C. K. Birdsall, J. Comput. Phys. **104**, 321 (1993).
[19]E. Kawamura, C. K. Birdsall, and V. Vahedi, Plasma Sources Sci. Technol. **9**, 413 (2000).
[20]H. C. Kim, O. V. Manuilenko, and J. K. Lee, "Particle-In-Cell Monte-Carlo Simulation of Capacitive RF Discharges: Comparison with Experimental Data, " Jpn. J. Appl. Phys. (to be published).
[21]J. R. M. Vaughan, IEEE Trans. Electron Devices **36**, 1963 (1989).
[22]J. R. M. Vaughan, IEEE Trans. Electron Devices **40**, 830 (1993).
[23]V. P. Gopinath, J. P. Verboncoeur, and C. K. Birdsall, Phys. Plasmas **5**, 1535 (1998).
[24]U. Buddemeier, U. Kortshagen, and I. Pukropski, Appl. Phys. Lett. **67**, 191 (1995).
[25]V. A. Godyak and R. B. Piejak, J. Appl. Phys. **82**, 5944 (1997).
[26]N. S. Yoon, S. S. Kim, C. S. Chang, and D. I. Choi, Phys. Rev. E **54**, 757 (1996).
[27]I. D. Kaganovich, Phys. Rev. Lett. **89**, 265006 (2002).
[28]V. A. Godyak and V. I. Kolobov, Phys. Rev. Lett. **79**, 4589 (1997).
[29]M. M. Turner, Phys. Rev. Lett. **75**, 1312 (1995).
[30]M. Surendra and D. B. Graves, Phys. Rev. Lett. **66**, 1469 (1991).
[31]V. A. Godyak and A. S. Khanneh, IEEE Trans. Plasma Sci. **14**, 112 (1986).
[32]S. V. Berezhnoi, I. D. Kaganovich, M. Misina, A. Bogaerts, and R. Gijbels, IEEE Trans. Plasma Sci. **27**, 1339 (1999).